Measurements of Mouse Pulmonary Artery Biomechanics

Naomi C. Chesler*
Department of Biomedical Engineering, University of Wisconsin, Madison, WI and Department of Mechanical Engineering, University of Vermont, Burlington, VT

John Thompson-Figueroa and Ken Millburne
Department of Internal Medicine, University of Vermont, Burlington, VT

Background: *Robust techniques for characterizing the biomechanical properties of mouse pulmonary arteries will permit exciting gene-level hypotheses regarding pulmonary vascular disease to be tested in genetically engineered animals. In this paper, we present the first measurements of the biomechanical properties of mouse pulmonary arteries.*
Method of Approach: *In an isolated vessel perfusion system, transmural pressure, internal diameter and wall thickness were measured during inflation and deflation of mouse pulmonary arteries over low (5-40 mmHg) and high (10-120 mmHg) pressure ranges representing physiological pressures in the pulmonary and systemic circulations, respectively.*
Results: *During inflation, circumferential stress versus strain showed the nonlinear "J"-shape typical of arteries. Hiidetz's incremental elastic modulus ranged from 27 ±13 kPa (n=7) during low-pressure inflation to 2,700 ±1,700 kP a (n=9) during high-pressure inflation. The low and high-pressure testing protocols yielded quantitatively indistinguishable stress-strain and modulus-strain results. Histology performed to assess the state of the tissue after mechanical testing showed intact medial and adventitial architecture with some loss of endothelium, suggesting that smooth muscle cell contractile strength could also be measured with these techniques.*
Conclusions: *The measurement techniques described demonstrate the feasibility of quantifying mouse pulmonary artery biomechanical properties. Stress-strain behavior and incremental modulus values are presented for normal, healthy arteries over a wide pressure range. These techniques will be useful for investigations into biomechanical abnormalities in pulmonary vascular disease.*
[DOI: 10.1115/1.1695578]

* Corresponding author: Department of Biomedica! Engineering, University of Wisconsin-Madison, 2146 Engineering Centers Building, 1550 Engineering Drive, Madison, WI 53706-1609. Phone: 608 265-8920; Fax: 608 265-9239; e-mail: Chesler@engr.wisc.edu.

Contributed by the Bioengineering Division for publication in the JOURNAL OF BIOMECHANICAL ENGINEERING, Manuscript received by the Bioengineering Division May 27, 2003; revision received September 23, 2003. Associate Editor: M. S. Sacks.

Introduction

Primary pulmonary hypertension (PPH) is a rapidly progressing and deadly disease that induces substantial pulmonary vascular remodeling [1]. Large and small pulmonary vessels exhibit thickening in all three layers of the blood vessel wall by both hypertrophy and hyperplasia of smooth muscle cells and by increased extracellular matrix protein deposition [2]. These biological changes have a significant effect on tissue biomechanical properties. For example, Young's modulus and residual stresses in rat pulmonary arteries have been shown to change with hypoxia-induced pulmonary hypertension [3,4]. Stress and strain distribution, compliance and impedance also have been estimated for the normal pulmonary vasculature of rats, cats, dogs, minipigs and newborn pigs [5–9]. However, there are no reported measurements of pulmonary artery biomechanical properties in mice.

Mice are useful models for studying diseases with known or suspected genetic defects since they are the only species for which genetically engineered mutants are widely available. For example, mice that have been genetically engineered to lack or over-express the gene for endothelial nitric oxide synthase are increasingly being used to study the effects of nitric oxide availability on the progression of hypoxia-induced pulmonary hypertension [10–12]. Furthermore, a genetic basis for many familial and sporadic cases of primary pulmonary hypertension has recently been discovered: heterozygous missense, nonsense and frameshift mutations in the bone morphogenetic protein type II receptor gene of the transforming growth factor beta cell-signaling superfamily [13,14]. Thus, the technical challenges of using such small animals for investigating pulmonary vascular remodeling are superseded by the exciting potential to explore molecular-level mechanisms in disease processes with genetically-engineered mice.

The goal of this study was to measure normal mouse pulmonary artery biomechanical properties in order to validate methods that could be applied to the pulmonary arteries of genetically engineered animals. Isolated vessel experiments were chosen for several reasons. First, this method allows good control of the mechanical environment, including transmural pressure, axial strain and vessel curvature. Also, since the vessel is isolated from its natural surroundings, the mechanical effects of tethering, which vary with vessel size and bifurcation level in the pulmonary vascular tree, can be neglected. Second, it allows excellent control of the biochemical environment, including pH, O_2, CO_2, temperature, and the absence of immunological or hormonal factors that could affect smooth muscle contraction or vascular tone. Finally, in arteries as small as the mouse pulmonary, the vessel inner diameter (ID) can be measured optically by transillumination. This well-described technique has led to many significant contributions in the field of resistance vessel physiology (for example, see [15–18]).

Materials and Methods

Left main pulmonary arteries were isolated from young (age: 7 weeks) C57BL6 mice after euthanasia as approved by the University of Vermont and University of Wisconsin Institutional Animal Care and Use Committees. The aorta, pulmonary veins, trachea, main bronchi and connective tissue were carefully removed after identification by specific anatomic location and morphology. The left pulmonary artery was then excised and mounted in an arteriograph chamber (Living Systems Instrumentation (LSI)). The arteriograph chamber consists of a bath for superfusion and a set of proximal and distal glass microcannulas (tip=400 μm) on which the artery is mounted and secured with single strands of nylon suture (diameter=10 μm). Thus mounted, vessels were perfused gently with Dulbecco's Modified Eagle's Medium (DMEM, Sigma Chemical Co.) through the proximal microcannula driven by a multi-roller pump. Pressure transducers were situated immediately up- and downstream of the vessel (P_{up} and P_{down}, respectively). An upstream in-line pressure servomechanism (LSI) continually adjusted the computed average transmural pressure (P_{ave} $= \frac{1}{2}(P_{up}+P_{down})$) via computer control (LabView, National Instruments). The distal microcannula was then closed off to flow and a static transmural pressure was applied to the vessels as previously described for rat middle cerebral arteries [19].

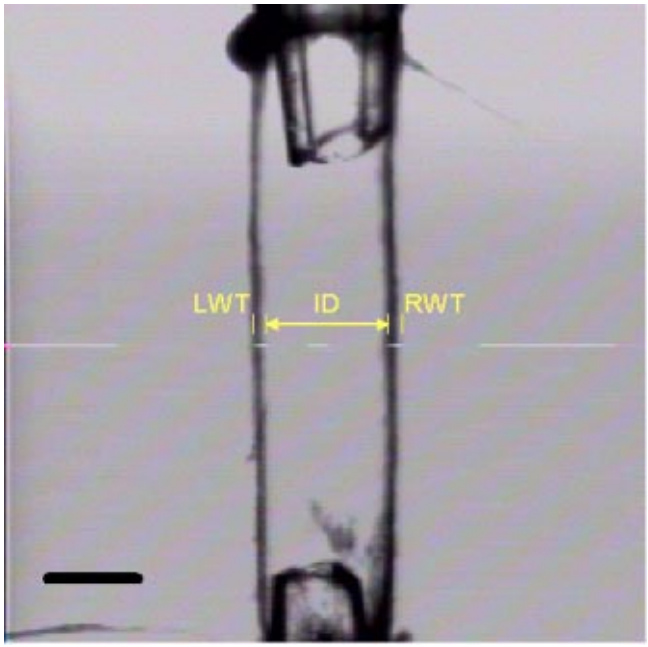

Fig. 1 Isolated mouse pulmonary artery sutured to glass microcannulas, pre-stretched and pressurized to 5 mmHg. The interrupted white line is the VDA scan-line, which shows the axial position of measurements. The short sections of the scan-line that overlap the vessel wall boundaries are the LWT and RWT measured by analog edge detection. ID is the distance between the inner boundaries of the detected walls (shown in yellow). Scale bar shows 400 μm.

The vessel was visualized through transillumination on an inverted microscope (CX40, Olympus) with a 10x objective. Through a trinocular observation tube with a 1.5x lens, the image was digitized in real time with a digital camera (C2020, Olympus). A video dimensional analyzer (VDA, LSI) electronically determined the ID and left and right wall thicknesses (LWT and RWT, respectively). Vessel dimensions were measured by the video scan line, which detects the optical contrast of the vessel wall and generates a voltage ramp within the VDA, the amplitude of which is proportional to length. A sample image with white scan line is shown in Fig. 1 for a vessel at 10 mmHg. The precision of the VDA is approximately ± 2.0 μm for this optical path after appropriate calibration. Inaccuracies can result from the artery centerline moving out of the plane of focus or loose connective tissue obscuring the edges of the vessel. The output of the VDA and up- and downstream pressure sensors were sent to a portable data acquisition computer (Latitude C800, Dell).

Two experimental protocols were used to measure tissue mechanical properties using a step history to approximate a constant load rate, as in [20]. These were low-pressure cyclic inflation and deflation (n=7) and high-pressure cyclic inflation and deflation (n=9) as detailed below. In particular, three of the vessels were subjected to the low-pressure protocol only, four were subjected to the low- and then the high-pressure protocol, and five were subjected to the high-pressure protocol only. No differences were observed between those vessels that were subjected to both the low and high-pressure protocols and those that were subjected to one only; thus, the data were grouped. In all cases, vessels were first slowly inflated to 40 mmHg (at approx. 10 mmHg/s) and pre-stretched so that no axial bending occurred at 40 mmHg. Typically, the amount of pre-stretch imposed was 50 to 100 μm, or

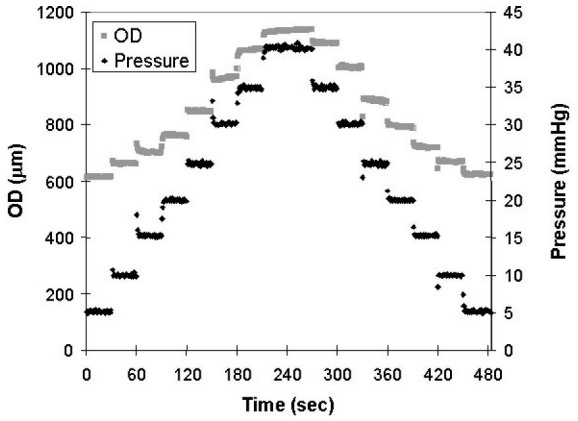

Fig. 2 Representative raw data for OD and P_{ave} versus time during the second cycle of the low pressure cyclic inflation/deflation protocol. Note occasional pressure over/undershoots during step changes, and some creep and creep recovery during inflation and deflation, respectively.

2.5% to 5%. Then, vessels were deflated and preconditioned with at least two cycles of low-pressure inflation and deflation identical to the low-pressure cyclic testing protocol. Tissue deformation in response to low-pressure inflation was consistent after the first cycle in general.

The peak pressure for the low-pressure protocol was chosen based on hypoxia-induced hypertensive pulmonary artery pressures in mice. The normal mean pulmonary artery pressure in C57BL6 wild type mice (20–30 g) is approximately 16 mmHg with peak systolic pressure up to 30 mmHg [21]. In response to hypoxia-induced hypertension, peak systolic pressure is 45 mmHg in the pulmonary circulation [10]. During low-pressure cyclic testing, average transmural pressure was stepped by 5 mmHg increments from 5 to 40 mmHg and then back down to 5 mmHg by 5 mmHg decrements five times in sequence, with each pressure held for 30 s (one minute at 40 mmHg). Five mmHg was chosen as the baseline pressure for this protocol since this was the lowest pressure at which vessels consistently did not collapse. Previous experiments on rat middle cerebral arteries were able to use baseline pressures closer to 0 mmHg [19]; however, the pulmonary arteries are relatively more thin-walled and thus more collapsible than cerebral arteries. The peak pressure for the high-pressure protocol was chosen based on normal systemic pressures in mice (peak systolic pressure is 120 mmHg [21]). During high-pressure inflation, pressure was incremented by 10 mmHg from 10 to 120 mmHg and decremented to 10 mmHg, with each pressure level held for one minute (two minutes at 120 mmHg). Axial bending was occasionally observed at the highest pressures.

P_{up}, P_{down} and average transmural pressure (P_{ave}), ID, LWT and RWT were sampled at 1 Hz and recorded continuously. Outer diameter (OD) was calculated as the sum of ID, LWT and RWT. Representative data for OD and P_{ave} during the second cycle of the low-pressure cyclic protocol are shown in Fig. 2. To compute static tissue behavior, data points collected midway through the constant-pressure step were used to control for the effects of the occasional pressure overshoot during the step increase and any viscoelastic effects. That is, for the low-pressure protocol, points were taken 15 s after the step change in pressure, and for the high-pressure protocol, points were taken 30 s after the step. Preliminary results demonstrated that with these protocols hysteresis was minimal between inflation and deflation, and no significant plastic deformation was evident.

After testing, mouse pulmonary arteries were preserved for histology to assess the state of the tissue after mechanical testing. Tissue was slow frozen in tissue freezing medium surrounded by 2-methyl butane cooled by liquid nitrogen. Thin sections (5–10 μm) were cut at -20°C on a cryostat (Richard-Allan Scientific) and stained with hematoxylin and eosin (Sigma Chemical Co.). Sections were imaged on an inverted microscope (TE-2000, Nikon) and captured using a spot camera and software for image capture and analysis (MetaVue, Optical Analysis Systems).

Calculations

The Cauchy stress in the circumferential direction was calculated at the inner wall using:

$$\sigma_\theta = \frac{P_{ave}(OD^2 + ID^2)}{OD^2 - ID^2} \tag{1}$$

[22] and the Almansi circumferential strain for large deformations using:

$$e_\theta = \frac{1}{2}\left(1 - \frac{1}{\lambda_\theta^2}\right) \tag{2}$$

[23] where the circumferential stretch ratio is $\lambda_\theta = \pi\ ID/\pi\ ID_0$ at the inner wall and ID_0 is the inner diameter at the baseline pressure. This approach is incrementally nonlinear in the sense that nonlinear effects due to large deformations are included and the material is only assumed to have a constant elastic modulus between states of incremental deformation.

An incremental elastic modulus developed by Hudetz [24] for arteries subjected to step changes in pressure at fixed length, which also assumes globally nonlinear, but incrementally linear behavior between adjacent states of deformation, was calculated using:

$$E_{inc} = \frac{\Delta P_{ave}}{\Delta ID}\frac{2ID\ OD^2}{OD^2 - ID^2} + \frac{2P_{ave}OD^2}{OD^2 - ID^2} \tag{3}$$

[24,25] where ΔP is an incremental change in average transmural pressure, ΔID is the corresponding change in internal diameter, and ID, OD and P_{ave} are taken at the beginning of the increment. This incremental elastic modulus calculation further assumes the wall material is orthotropic, incompressible and homogeneous. In the absence of reliable residual stress (opening angle) and longitudinal force data, parameters for a fully three-dimensional model of tissue mechanics (such as have been suggested in the literature and concisely reviewed in [26]) were not estimated.

Results

Pulmonary artery arterial diameter increased and decreased sigmoidally in response to increasing and decreasing transmural pressures for the low-pressure cycles (Fig. 3*a*). At the initial pressure of 5 mmHg, the OD was 628 ± 39 μm and ID/WT was 7 ± 4. At the highest pressure of 40 mmHg, the vessels dilated to 1183 ± 58 μm OD with ID/WT equal to 23 ± 5. In response to increasing and decreasing transmural pressures for the high-pressure cycles, the diameter increased and decreased roughly logarithmically (Fig. 3*b*). At the initial pressure of 10 mmHg, the average OD was 638 ± 50 μm and ID/WT was 7 ± 4; at the highest pressure of 120 mmHg, the vessels dilated to 1258 ± 73 μm with ID/WT equal to 30 ± 8.

The stress-strain behavior of the arteries in both pressure groups showed the "J"-shape typical of arteries (Fig. 4*a*). E_{inc} also increased with increasing strain with a "J"-shape during inflation in both pressure groups (Fig. 4*b*). For both calculations, the low- and high-pressure testing protocols yielded quantitatively indistinguishable results where the strain values overlapped.

Hematoxylin and eosin staining showed some intact endothelial cells and many medial smooth muscle and adventitial fibroblast cells in a representative mechanically tested artery (Fig. 5).

Discussion

Synchronous pressure-diameter measurements in an isolated vessel perfusion system were used to quantify the biomechanical properties of normal, healthy mouse pulmonary arteries. Diameter

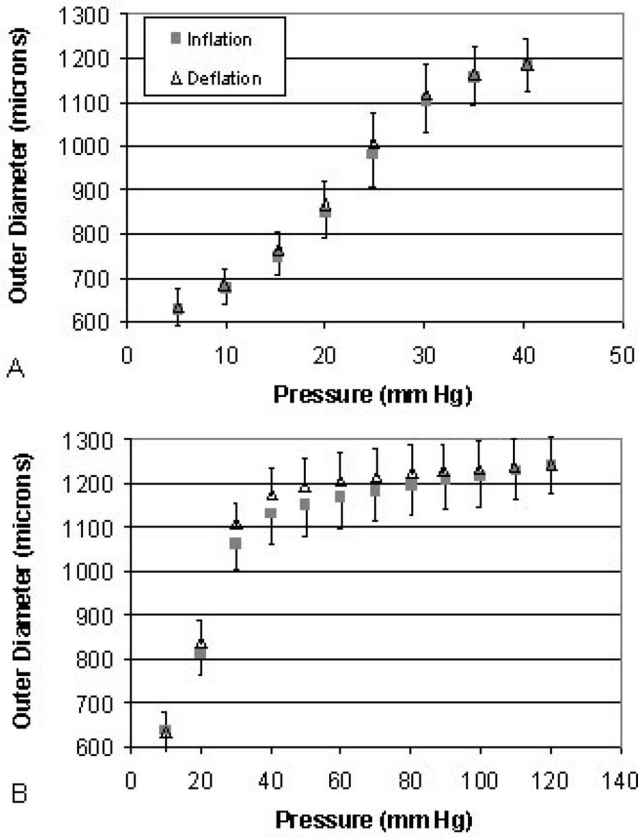

Fig. 3 Outer diameter versus pressure for (*a*) low and (*b*) high pressure inflation (gray boxes) and deflation (open triangles) of isolated left main pulmonary arteries. Values are mean ±SD (−SD for inflation, +SD for deflation).

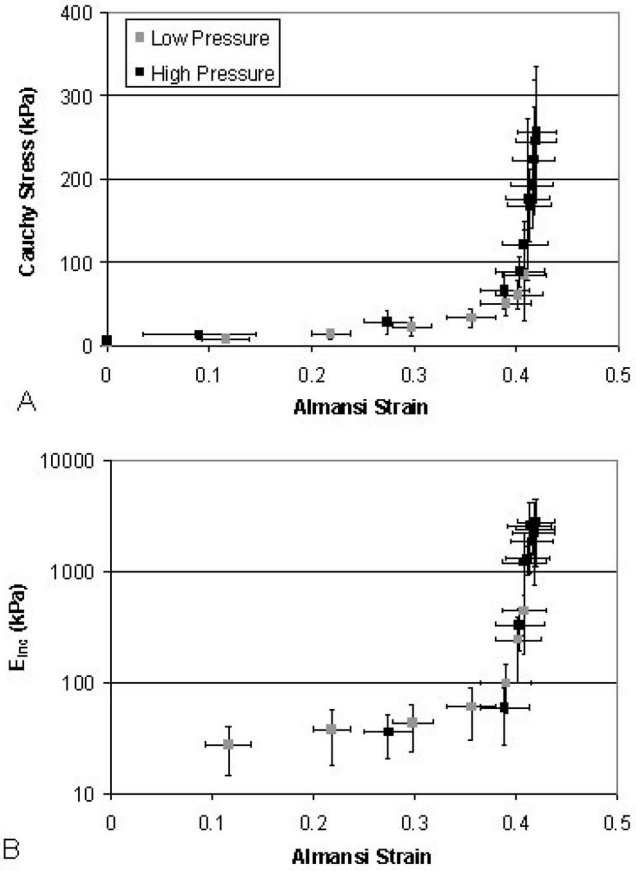

Fig. 4 (*a*) Cauchy stress and (*b*) Hudetz's incremental elastic modulus versus Almansi strain during inflation for low pressure (gray boxes) and high pressure (black boxes) testing protocols. Values are mean ±SD, with E_{inc} values on a log scale.

change as a function pressure was sigmoidal in shape, as has been observed in other vessel types [20,27–29]. Langewouters and coauthors, in particular, used a three-parameter arctangent function to describe the outer cross-sectional area change of human aorta subjected to an inflation and deflation protocol similar to ours [20]. We used this arctangent function to model our pressure-diameter data and obtained comparable parameter values for the low and high-pressure groups with good degrees of fit (data not shown).

Stress-strain behavior and the incremental modulus with respect to strain were calculated to characterize the mouse pulmonary artery elastic behavior. E_{inc} values ranged from 27±13 kPa during low-pressure inflation to 2,700±1,700 kPa during high-pressure inflation. These data fall well within the range of E_{inc} values reported in the literature for other vessel types [24,25,30–33]. In particular, in rat middle cerebral arteries with experimental and analytical methods identical to those used here, E_{inc} increased from 25 to 3,667 kPa with increasing pressure from 5 to 150 mmHg [25]. The shapes of the stress-strain and E_{inc}-strain relationships are consistent with a two component model of the artery where the low modulus properties of elastin dominate at low stretch and high modulus recruited collagen fibers dominate at high stretch. The pattern of variation of E_{inc} with strain or pressure may be a useful indicator of vessel structural composition, and may change significantly with vascular remodeling [32].

Histology on a representative mouse pulmonary artery demonstrated intact medial and adventitial cells and architecture with some endothelial cell stripping. Endothelial cells are not expected to contribute significantly to arterial mechanical properties, but their absence suggests that assays for vessel reactivity that rely on an intact endothelium should not be pursued. In contrast, the collagen-rich adventitia is expected to contribute to tissue mechanical properties. Indeed, the relatively equal sizes of the media and adventitia support our conjecture above that collagen plays a significant role in pulmonary artery biomechanical properties. The presence of ample smooth muscle cells suggests that contractile strength could be measured with the techniques presented here by adding to the bath vasoconstrictors such as norepinephrine and potassium chloride, or vasodilators such as sodium nitroprusside and papaverine, as described with other vessel types [25].

Limitations of the isolated vessel technique with mouse pulmonary arteries include experimental error in the transillumination measurements, in particular LWT and RWT. At the highest pressures, the wall thicknesses are small but have sharp contrast with the surrounding fluid. As the pressure decreases, the walls thicken and lose the sharply defined contrast that is easily detectable optically. Our data from the low (high)-pressure testing protocol diverge on average 20% (15%) from the incompressible, constant axial length assumption. A solution to this problem suggested by Faury et al. is to measure the wall thickness optically at the highest pressure and then compute average wall thickness at lower pressures based on conservation of wall cross-sectional area (that is, assuming incompressibility and no axial strain) [34]. The assumption of zero axial strain is reasonable since the total suture-to-suture vessel length is fixed (suture slippage would catastrophically end the experiment), but some changes in the distribution of axial strain may occur. The absence of a local axial strain measurement is another limitation of this study. Differences in axial strain between normal and transgenic mice may be an important measure of the functional effects of the transgene in the vasculature.

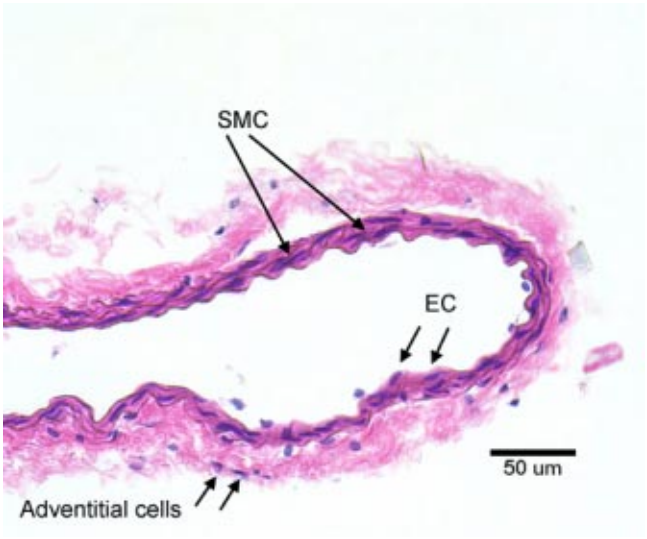

Fig. 5 Representative mouse pulmonary artery in cross-section stained with hematoxylin and eosin. Intact medial smooth muscle cells (SMC) and adventitial cells are visible; a few intact endothelial cells (EC) are visible.

Also, we were not able to measure pulmonary artery length in vivo and so were not able to mount the vessels at their in vivo length. However, with arteries mounted in the system as described above, we performed low-pressure cyclic inflation/deflation testing at three levels of axial extension (20, 40 and 60 μm, representing approximately 2% to 6% axial stretch) past the pre-stretched length and did not see differences in deformation (data not shown). Stretch ratios on the order 1.4 to 1.7, as suggested by Huang et al. [4] for pulmonary arterial segments from rats, resulted in the vessel detaching from the microcannulas. If the vessels are understretched axially as compared to the in vivo condition, the measured deformations most likely overestimate, and incremental moduli underestimate, the in vivo response. Finally, given the small aspect ratio (length/width) of these vessels when cannulated (see Fig. 1), and especially when pressurized, end effects may have influenced the measured properties. At the highest pressures tested, the aspect ratio fell as low as 1.5 in some cases.

In these experiments, we have measured the biomechanical properties of isolated mouse pulmonary arteries and described their behavior over a wide pressure range. The techniques to quantify stress-strain and modulus-strain relationships described here serve as a basis for experiments to quantify the biomechanical aspects of pulmonary vascular remodeling in mice. In the future, these methods could be applied to the pulmonary vasculature of genetically-engineered mice to investigate gene-level molecular mechanisms in pulmonary vascular remodeling, which may be applicable to pulmonary vascular disease in humans.

Acknowledgments

Funding support from NIH COBRE grant P20RR15557 is gratefully acknowledged. The authors also wish to thank Daniel Sidney, Ray Vanderby, Rod Lakes and Ryan Kobs for helpful discussions.

References

[1] Gaine, S. P., and Rubin, L. J., 1998, "Primary Pulmonary Hypertension [Published Erratum Appears in Lancet 1999 Jan 2;353(9146):74]," Lancet, **352**(9129), p. 719–25.
[2] Jeffery, T. K., and Wanstall, J. C., 2001, "Pulmonary Vascular Remodeling: A Target for Therapeutic Intervention in Pulmonary Hypertension," Pharmacological Therapies, **92**(1), p. 1–20.
[3] Huang, W., Sher, Y. P., Delgado-West, D., Wu, J. T., Peck, K., and Fung, Y. C., 2001, "Tissue Remodeling of Rat Pulmonary Artery in Hypoxic Breathing. I. Changes of Morphology, Zero-Stress State, and Gene Expression," Ann. Biomed. Eng., **29**(7), p. 535–51.
[4] Huang, W., Delgado-West, D., Wu, J. T., and Fung, Y. C., 2001, "Tissue Remodeling of Rat Pulmonary Artery in Hypoxic Breathing. II. Course of Change of Mechanical Properties," Ann. Biomed. Eng., **29**(7), p. 552–62.
[5] Chen, E. P., Bittner, H. B., Craig, D. M., Davis, Jr., R. D., and Van Trigt, 3rd, P., 1997, "Pulmonary Hemodynamics and Blood Flow Characteristics in Chronic Pulmonary Hypertension," Ann. Thorac. Surg., **63**(3), p. 806–13.
[6] Domkowski, P. W., Messier, Jr., R. H., Cockerham, J. T., Kot, P. A., Diodato, L. H., and Hopkins, R. A., 2001, "Relationship of Hydraulic Impedance and Elasticity in the Pulmonary Artery of Maturing Newborn Pigs," J. Surg. Res., **100**(1), p. 116–26.
[7] Segers, P., Brimioulle, S., Stergiopulos, N., Westerhof, N., Naeije, R., Maggiorini, M., and Verdonck, P., 1999, "Pulmonary Arterial Compliance in Dogs and Pigs: The Three-Element Windkessel Model Revisited," Am. J. Physiol., **277**(2 Pt 2), p. H725–31.
[8] Yen, R. T., Fung, Y. C., and Bingham, N., 1980, "Elasticity of Small Pulmonary Arteries in the Cat," J. Biomech. Eng., **102**(2), p. 170–7.
[9] Zhao, J., Day, J., Yuan, Z. F., and Gregersen, H., 2002, "Regional Arterial Stress-Strain Distributions Referenced to the Zero-Stress State in the Rat," American Journal of Physiology-Heart & Circulatory Physiology, **282**(2), p. H622–9.
[10] Fagan, K. A., Fouty, B. W., Tyler, R. C., Morris, Jr., K. G., Hepler, L. K., Sato, K., LeCras, T. D., Abman, S. H., Weinberger, H. D., Huang, P. L., McMurtry, I. F., and Rodman, D. M., 1999, "The Pulmonary Circulation of Homozygous or Heterozygous eNOS-Null Mice Is Hyperresponsive to Mild Hypoxia," J. Clin. Invest., **103**(2), p. 291–9.
[11] Fagan, K. A., Tyler, R. C., Sato, K., Fouty, B. W., Morris, Jr., K. G., Huang, P. L., McMurtry, I. F., and Rodman, D. M., 1999, "Relative Contributions of Endothelial, Inducible, and Neuronal NOS to Tone in the Murine Pulmonary Circulation," Am. J. Physiol., **277**(3 Pt 1), p. L472–8.
[12] Yamashita, T., Kawashima, S., Ohashi, Y., Ozaki, M., Rikitake, Y., Inoue, N., Hirata, K., Akita, H., and Yokoyama, M., 2000, "Mechanisms of Reduced Nitric Oxide/cGMP-Mediated Vasorelaxation in Transgenic Mice Overexpressing Endothelial Nitric Oxide Synthase," Hypertension, **36**(1), p. 97–102.
[13] Thomson, J. R., Machado, R. D., Pauciulo, M. W., Morgan, N. V., Humbert, M., Elliott, G. C., Ward, K., Yacoub, M., Mikhail, G., Rogers, P., Newman, J., Wheeler, L., Higenbottam, T., Gibbs, J. S., Egan, J., Crozier, A., Peacock, A., Allcock, R., Corris, P., Loyd, J. E., Trembath, R. C., and Nichols, W. C., 2000, "Sporadic Primary Pulmonary Hypertension Is Associated with Germline Mutations of the Gene Encoding BMPR-II, a Receptor Member of the TGF-beta Family," J. Med. Genet., **37**(10), p. 741–5.
[14] Machado, R. D., Pauciulo, M. W., Thomson, J. R., Lane, K. B., Morgan, N. V., Wheeler, L., Phillips, 3rd, J. A., Newman, J., Williams, D., Galie, N., Manes, A., McNeil, K., Yacoub, M., Mikhail, G., Rogers, P., Corris, P., Humbert, M., Donnai, D., Martensson, G., Tranebjaerg, L., Loyd, J. E., Trembath, R. C., and Nichols, W. C., 2001, "BMPR2 Haploinsufficiency as the Inherited Molecular Mechanism for Primary Pulmonary Hypertension," Am. J. Hum. Genet., **68**(1), p. 92–102.
[15] Mulvany, M. J., and Halpern, W., 1977, "Contractile Properties of Small Arterial Resistance Vessels in Spontaneously Hypertensive and Normotensive Rats," Circ. Res., **41**(1), p. 19–26.
[16] Warshaw, D. M., Mulvany, M. J., and Halpern, W., 1979, "Mechanical and Morphological Properties of Arterial Resistance Vessels in Young and Old Spontaneously Hypertensive Rats," Circ. Res., **45**(2), p. 250–9.
[17] Cipolla, M. J., Harker, C. T., and Porter, J. M., 1996, "Endothelial Function and Adrenergic Reactivity in Human Type-II Diabetic Resistance Arteries," J. Vasc. Surg., **23**(5), p. 940–9.
[18] Mandala, M., Gokina, N., and Osol, G., 2002, "Contribution of Nonendothelial Nitric Oxide to Altered Rat Uterine Resistance Artery Serotonin Reactivity During Pregnancy," Am. J. Med. Electron., **187**(2), p. 463–8.
[19] Coulson, R. J., Cipolla, M. J., Vitullo, L., and Chesler, N. C., 2004, "Mechanical Properties of Rat Middle Cerebral Arteries (NOS 3) With and Without Myogenic Tone," J. Biomech. Eng. **126**(1), p. 76–81.
[20] Langewouters, G. J., Wesseling, K. H., and Goedhard, W. J., 1984, "The Static Elastic Properties of 45 Human Thoracic and 20 Abdominal Aortas in Vitro and the Parameters of a New Model," J. Biomech., **17**(6), p. 425–35.
[21] Steudel, W., Ichinose, F., Huang, P. L., Hurford, W. E., Jones, R. C., Bevan, J. A., Fishman, M. C., and Zapol, W. M., 1997, "Pulmonary Vasoconstriction and Hypertension in Mice with Targeted Disruption of the Endothelial Nitric Oxide Synthase (NOS 3) Gene," Circ. Res., **81**(1), p. 34–41.
[22] Timoshenko, S., 1934, Theory of Elasticity. First ed. 1934, New York, NY: McGraw-Hill Book Company, Inc.
[23] Fung, Y. C., 1990, Biomechanics: Motion, Flow, Stress and Growth. 1990, New York City: Springer-Verlag New York Inc.
[24] Hudetz, A. G., 1979, "Incremental Elastic Modulus for Orthotropic Incompressible Arteries," J. Biomech., **12**(9), p. 651–5.
[25] Coulson, R. J., Chesler, N. C., Vitullo, L., and Cipolla, M. J., 2002, "Effects of Ischemia and Myogenic Activity on Active and Passive Mechanical Properties of Rat Cerebral Arteries," American Journal of Physiololgy: Heart and Circulation Physiolology, **283**(6), p. H2268–75.
[26] Humphrey, J. D., 1999, "An Evaluation of Pseudoelastic Descriptors Used in Arterial Mechanics," J. Biomech. Eng., **121**(2), p. 259–62.
[27] Kornet, L., Jansen, J. R., Nijenhuis, F. C., Langewouters, G. J., and Versprille, A., 1998, "The Compliance of the Porcine Pulmonary Artery Depends on Pressure and Heart Rate," J. Physiol. (London), **512**(Pt 3), p. 917–26.
[28] Caputo, L., Tedgui, A., Poitevin, P., and Levy, B. I., 1992, "In Vitro Assess-

ment of Diameter-Pressure Relationship in Carotid Arteries from Normotensive and Spontaneously Hypertensive Rats," J. Hypertens. Suppl., 10(6), p. S27-30.
[29] Stefanadis, C., Demellis, J., Tsiamis, E., Diamantopoulos, L., Michaelides, A., and Toutouzas, P., 2000, "Assessment of Aortic Line of Elasticity Using Polynomial Regression Analysis," Circulation, 101(15), p. 1819-25.
[30] Hayashi, K., Handa, H., Nagasawa, S., Okumura, A., and Moritake, K., 1980, "Stirfness and Elastic Behavior of Human Intracranial and Extracranial Arteries," J. Biomech., 13(2), p. 175-84.
[31] Bank, A. J., Wang, H., Holte, J. E., Mullen, K., Shaimnas, R., and Kubo, S. H., 1996, "Contribution of Collagen, Elastin, and Smooth Muscle to in Vivo Human Brachial Artery Wall Stress and Elastic Modulus," Circulation, 94(12), p. 3263-70.
[32] Zulliger, M. A., Montorzi, **G., and** Stergiopulos, N., 2002, "Biomechamcal Adaptation of Porcine Carotid Vascular Smooth Muscle to Hypo and Hypertension in Vitro," J. Biomech., 35(6), p. 757-65.
[33] Hayashi, K., Takamizawa, K., Nakamura, T, Kato, T., and Tsushima, N., 1987, "Effects of Elastase on the StifTness and Elastic Properties of Arterial Walls in Cholesterol-Fed Rabbits," Atherosclerosis, 66(3), p. 259-67.
[34] Faury, G., Maher, G. M., Li, D. Y., Keating, M. T., Mecham, R. P., and Boyle, W. A., 1999, "Relation between Outer and Luminal Diameter in Cannulated Arteries," Am. J. Physiol., 277(5 Pt 2), p. H1745-53.

